3d nonlocal simulation of ductile crack growth — a numerical realization

Herbert Baaser — Dietmar Gross

Institute of Mechanics, Darmstadt University of Technology
Hochschulstrasse 1, D–64289 Darmstadt, Germany
baaser@mechanik.tu-darmstadt.de

ABSTRACT. *In this article we present a realization of a three dimensional ductile damage analysis. The* ROUSSELIER *model is used in a finite strain formulation to represent the material behavior, so that a threshold value of the damage parameter β, which corresponds to an assumed void volume fraction, can be defined as crack propagation criterion. We propose a new solution approach using a nonlocal damage formulation in the scope of the finite element method. This approach uses a set of constitutive equations with a* BAŽANT*–type nonlocal regularization and an iterative* NEWTON–RAPHSON*–scheme, which requires the determination of the global stiffness matrix and the residuum vector of the system by the assembling of local solutions in each integration point. For the spatial discretization 20–nodes–brick elements with $2 \times 2 \times 2$–integration are used. A numerical example shows the applicability of the new solution algorithm.*

RÉSUMÉ. *Dans cet article on présente une analyse tridimensionelle de l'endommagement ductile. Le modèle de* ROUSSELIER *est utilisé en grandes déformations pour représenter le comportement du matériau, de sorte qu'une valeur critique de la variable endommagement β est utilisée comme critère de propagation. On propose une nouvelle solution utilisant une formulation non locale dans le cadre d'une modélisation par éléments finis. Cette approche utilise des équations constitutives avec une régularisation non locale de type* BAŽANT *associée à une stratégie de résolution itérative par un schéma de* NEWTON–RAPHSON*. Celle–ci nécessite la détermination de la matrice globale tangente et du vecteur second–membre par assemblage de solutions locales en chaques points d'intégration. Pour la discrétisation spatiale des éléments octaédriques à 20 nœuds et $2 \times 2 \times 2$ points d'intégration sont utilisés. Des exemples numériques illustrent les possibilités du nouvel algorithme.*

KEY WORDS: *3D–Finite–Element–Simulation, Finite Strain Plasticity, Ductile Damage, Nonlocal Regularization*

MOTS-CLÉS : *Eléments finis 3D, plasticité en grandes déformations, endommagement ductile, regularisation non locale*

REEF – 10/2001. NUMEDAM'00, pages 353 to 367

1. Introduction

Many structural parts of technical applications require a detailed computational analysis of their load carrying capacity either during the design phase or later on while operating in a larger system or in a machine. Today a computational evaluation and simulation of such structural parts is also able to consider the influence of damage and failure occurance by continuum damage models implemented in the framework of the FEM. A well–known disadvantage in the numerical treatment of solid mechanics problems, where softening material behavior occurs, is the so–called *mesh–dependence* of numerical results. In a considerable number of investigations different methods have been proposed to overcome the mesh–dependence of finite element results. The common idea is the introduction of a *characteristic* or *internal* length (scale) into the constitutive model or its evaluation. We mention four different types of models. A type of COSSERAT models consider in addition to the displacement of a material point also its rotation as independent kinematic variable, see [EHL 98]. The internal length introduced by this was shown to determine the width of shear bands especially in soil materials, where the additional rotational degrees of freedom are activated during the deformation history. For such shear dominated problems this method seems to be a suitable regularization technique. Another advanced regularization method is the introduction of higher displacement gradients as additional degrees of freedom. A consistent formulation in terms of small–strains is available, see e.g. [BOR 99]. A totally different approach to model the failure occurrence is the discrete representation of the actual failure or damage mode. Such models are able to represent failure occurrence by special finite elements either capable of showing displacement jumps internally within the element structure, see [OLI 96], or between the element edges through a specific *cohesive* law defining the stress–strain behavior, see e.g. [HOH 96] or [BAA 97]. Another type of regularizing approaches is known as *non–local*, based on a spatial smoothing of certain quantities over the volume or structure of interest, see [BAŽ 88]. The main goal of this type of model is an additional evaluation of a volume integral for the internal variables like plastic strain or damage, convoluted e.g. by a bell–like kernel function, see [PIJ 93]. Many authors used this smoothing technique like [LEB 94], [TVE 97] or [BAA 98]. They computed the smoothing of the damage parameter as an additional process applied on the actual result of the local solution of the constitutive equations. In this paper we describe a new approach of evaluating the volume integral for the increment of the damage parameter used. The idea is to compute the smoothing during the iteration of the set of constitutive equations, which is advantageous due to the iterative character of the equation solver applied. In this study 20–noded brick 3D elements are used with quadratic shape functions along the element edges. [MAT 94] have found that this element type well represents localization in the 3D case. As constitutive model we use the ductile damage model of [ROU 89]. An advantage of this model is the description of material softening behavior due to damage by the influence of just three material parameters. Nevertheless, there are only a few articles treating the calibration of the ROUSSELIER parameters to experimental data, see [ROU 89] and [LI 94]. A second advantage is related to the numerical implementation of the constitutive law by means of an implicit integration scheme. The

type of constitutive equations leads to symmetric tangent material moduli, which is advantageous in computing and storing the matrix expressions.

2. Nonlinear solution & nonlocal formulation

2.1. *Classical iterative solution procedure*

In order to approximate the real nonlinear behavior of a structure, the final load, leading to an unknown displacement result $\mathbf{u}$, is usually divided into smaller load steps. Thus, for each load level the structural response is computed by finding the actual equilibrium, using an iterative solution procedure. The accumulation of the incremental solutions $\Delta\mathbf{u}$ of the displacement field results in the total answer $\mathbf{u}$.

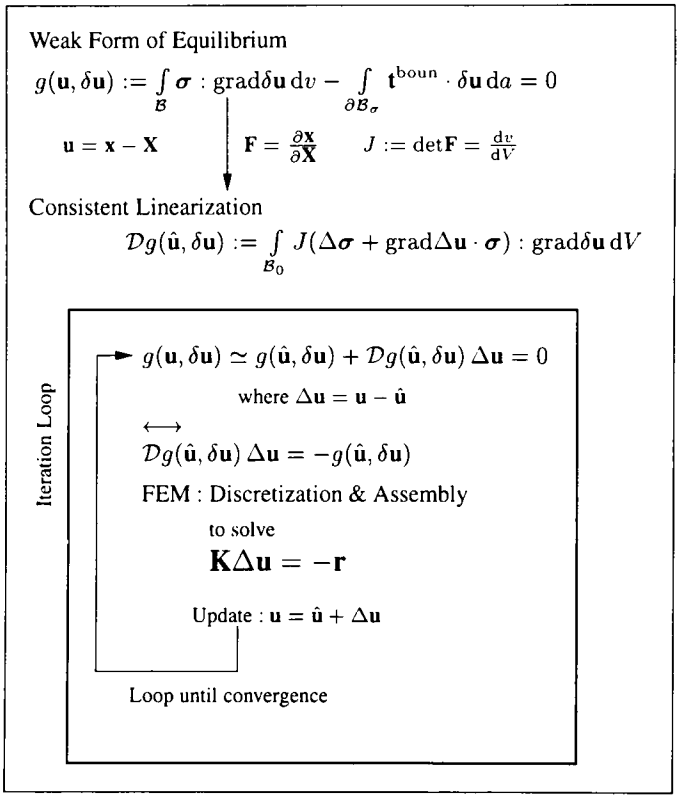

FIG. 1. *Classical iterative FEM solution procedure for a given load level*

Starting from the weak form of equilibrium $g(\mathbf{u},\delta\mathbf{u}) = 0$, where $\delta\mathbf{u}$ indicates the vector of test functions which is identified with the virtual displacements, an iterative solution method can be constructed to determine for the unknown displacements $\mathbf{u}$ at

a given load, with prescribed boundary displacements $\bar{\mathbf{u}}$. The displacements describe the difference between the current and the initial configuration by $\mathbf{u} = \mathbf{x} - \mathbf{X}$. The representation of $g(\mathbf{u}, \delta\mathbf{u}) = 0$ in terms of a TAYLOR–series from a known position $\hat{\mathbf{u}}$ with $\Delta\mathbf{u} = \mathbf{u} - \hat{\mathbf{u}}$ leads to a first order approximation of the weak form. This expression is the basis for the *global* iteration loop to find the increments $\Delta\mathbf{u}$ and thus the new displacements $\mathbf{u}$. This procedure is schematically described in Fig. 1, where $\mathcal{B}$ describes the considered body in the current configuration with the volume v and with $\mathbf{t}^{boun}$ as traction vector applied on the boundary $\partial\mathcal{B}_\sigma$. In the next load step the new solution of the system has to be determined by repeating this iteration.

2.2. *Nonlocal formulation*

In the usual iterative procedures all quantities are stored locally on the level of integration points. However, the nonlocal approach which is proposed here, acts on the level of internal quantities on the integrations points. [BAŽ 88] have shown that a nonlocal treatment of the damage quantities leads to mesh–insensitivity. For this purpose we apply the nonlocal smoothing integral to the increment $\Delta\beta$ of ROUSSELIERs damage quantity

$$\Delta\beta^{nonloc}(\mathbf{X}) = \frac{\displaystyle\int_{\mathcal{B}_0} \Delta\beta^{local}(\mathbf{s})\, \varphi(\mathbf{S} - \mathbf{X})\, \mathrm{d}V(\mathbf{S})}{\displaystyle\int_{\mathcal{B}_0} \varphi(\mathbf{S} - \mathbf{X})\, \mathrm{d}V(\mathbf{S})} \qquad [1]$$

where the kernel function, chosen as

$$\varphi(\mathbf{p}) = \exp\left[-\frac{k^2}{l_c^2}\mathbf{p}\cdot\mathbf{p}\right], \qquad [2]$$

for an arbitrary position vector $\mathbf{p}$ is responsible for the nonlocal smoothing of the local quantity $\Delta\beta^{local}$ with respect to the reference state $\mathbf{X}$. Formally the characteristic length l_c describes the standard deviation of the normal distribution. For a discussion of the factor k depending on the spatial dimension of the problem considered see [BAŽ 88]. Following their arguments $k \equiv (6\sqrt{\pi})^{1/3} \simeq 2.2$ for the 3D case considered here. For the numerical implementation the volume integral [1] is applied for each integration point considering just the surrounding by a sphere of radius $3l_c$, which is sufficient for a tolerable integration error in this application. A possible crossing of symmetry lines or planes during the integration loop is respected by accounting for the *virtual* contributions of the volume integration. But the whole computation of the respective influence of the neighbourhood of each integration point can be calculated once as a preprocessing procedure and takes just a few minutes for the considered problems. The main issue of the new solution algorithm is the assembling of the global stiffness matrix and the global residual vector. In Fig. 1 the global equilibrium iteration is illustrated, with the use of the residual $g(\mathbf{u}, \delta\mathbf{u})$ and the actual system stiffness $\mathcal{D}g(\hat{\mathbf{u}}, \delta\mathbf{u})$. In the FE representation the quantity $g(\mathbf{u}, \delta\mathbf{u})$ results in the residual vector

and the system stiffness $\mathcal{D}g(\hat{\mathbf{u}}, \delta\mathbf{u})$ in the global stiffness matrix, respectively. During the assembling procedure for these terms the actual increments for the local description of the constitutive behavior are computed. The numerical procedure for this kind of solution is described in the Appendix (see eqn. [23]), where the calculation of the local solution of the constitutive equations is demonstrated. In contrast, the new idea consists in a *global* computation of the increments $\Delta\mathbf{x}$ in [23] by a NEWTON–like iteration scheme. The specific algorithmic treatment of this iteration is described shortly in Section [4.2] and in an earlier version in [BAA 00]. Due to the iterative character of the new solving scheme it is possible to modify the actual solution of the increment of the damage parameter β by a *nonlocal* approach. This modification is not possible in the traditional iterative solution procedure, where the evaluation of the constitutive equations is treated in each integration point violating the yield condition, without considering its spatial position. On the contrary with this new approach a "communication" between the integration points is enabled due to eqn. [1], where the local increment of the damage parameter is modified depending on its location. The described nonlocal modification of the increment $\Delta\beta$ of the damage parameter influences the solution convergence of the set of constitutive equations, but this *intervention* acts in a moderate way so that convergence is obtained. In contrast to the method described e.g. in [BAA 98], we here operate *in small steps*, which influences the solution of the constitutive equations by the nonlocal character, but guarantees the global quadratic convergence behavior.

3. Finite strain plasticity and damage model

3.1. *Finite strain plasticity*

In elastic–plastic solids under sufficiently high load finite deformations occur, where the plastic part of the strains usually is large compared with the elastic part. The description of finite plastic deformations in conjunction with damage models is often done by using the additive decomposition of the elastic and plastic strains rates, [TVE 89]. Here however, we use the framework of multiplicative elastoplasticity which is widely accepted in plasticity. Its kinematic key assumption is the multiplicative split of the deformation gradient

$$\mathbf{F} = \mathbf{F}_{el} \cdot \mathbf{F}_{pl} \qquad [3]$$

into an elastic and a plastic part, providing the basis of a geometrically exact theory and avoiding linearization of any measure of deformation. As a further advantage, fast and numerically stable iterative algorithms, proposed and described by [SIM 92], can be used. In the following, only a brief summary of the algorithm in the context of a FE–implementation is given.

An essential aspect of [3] is the resulting additive structure of the current logarithmic principal strains within the return mapping scheme as

$$\epsilon^{el} = \epsilon^{tr} - \Delta\epsilon^{pl} \,. \qquad [4]$$

Here, $\epsilon_i = \ln \lambda_i$ $(i = 1, 2, 3)$ and λ_i^2 are the eigenvalues of an elastic trial state, described by the left CAUCHY–GREEN tensor $\mathbf{b}_{el}^{tr}$. The elastic strains ϵ^{el} are defined by HOOKE's law and the plastic strain corrector $\Delta\epsilon^{pl}$ can be derived by the normality rule of plastic flow. The elastic left CAUCHY–GREEN tensor can be specified with the decomposition [3] as

$$\mathbf{b}_{el} = \mathbf{F}_{el} \cdot \mathbf{F}_{el}^{\mathrm{T}} = \mathbf{F} \cdot \mathbf{C}_{pl}^{-1} \cdot \mathbf{F}^{\mathrm{T}} \,, \qquad [5]$$

which clearly shows the "connection" between the elastic and plastic deformation measure by the occurance of the plastic right CAUCHY–GREEN tensor $\mathbf{C}_{pl} = \mathbf{F}_{pl}^{\mathrm{T}} \cdot \mathbf{F}_{pl}$. By means of the relative deformation gradient (see [SIM 92])

$$\mathbf{f} = \frac{\partial \mathbf{x}}{\partial \mathbf{x}_{n-1}} = \mathbf{F} \cdot \mathbf{F}_{n-1}^{-1} \,, \qquad [6]$$

which relates the current configuration $\mathbf{x}$ to the configuration belonging to the previous time step at t_{n-1}, an elastic *trial*–state is calculated for the current configuration at time t_n

$$\mathbf{b}_{el}^{tr} = \mathbf{f} \cdot \mathbf{b}_{n-1} \cdot \mathbf{f}^{\mathrm{T}} \qquad [7]$$

with frozen internal variables at state t_{n-1}. If the condition $\Phi \leq 0$ (see eqn. [10]) is fulfilled by the current stress state $\boldsymbol{\tau}$, this state is possible and is the solution. If, on the other hand, $\Phi \leq 0$ is violated by the trial–state, the trial stresses must be projected back on the yield surface $\Phi = 0$ in an additional step. This "return mapping" procedure is used as the integration algorithm for the constitutive equations described in Section 3.2. It should be mentioned that the algorithmic treatment in terms of principal axes has some advantages concerning computational aspects like time and memory saving. Based on this, the integration procedure of the constitutive equations for large and for small deformations is very similar, [ARA 87].

3.2. *The Rousselier damage model*

First, some notations and characters, which will be used in this description of the constitutive law and later on in the algorithmic setting, are specified. Following the ideas of [ARA 87] we decompose the stress and strain tensors in scalar values, which is of great advantage for the numerical implementation. Thus, we write the KIRCHHOFF stress tensor $\boldsymbol{\tau}$ as weighted CAUCHY stress tensor as follows

$$\boldsymbol{\tau} = J\,\boldsymbol{\sigma} = -p\mathbf{1} + \frac{2}{3} q \mathbf{n}^{\tau} \,, \qquad [8]$$

where $J := \det \mathbf{F} = \frac{\mathrm{d}v}{\mathrm{d}V} = \frac{\rho_0}{\rho}$ and $p = -\frac{1}{3}\tau_{ij}\delta_{ij}$ defines the hydrostatic pressure, $q = \sqrt{\frac{3}{2} t_{ij} t_{ij}}$ the equivalent stress and $t_{ij} = \tau_{ij} + p\delta_{ij}$ are the components of the stress deviator. In this notation an additional important quantity is the normalized

stress deviator $\mathbf{n}^T = \frac{3}{2q}\mathbf{t}$. The second order identity tensor $\mathbf{1}$ is defined as the KRONECKER symbol by its components δ_{ij} in the cartesian frame. In an analogous way the plastic strain rate can be written as

$$\Delta\boldsymbol{\epsilon}^{pl} = \frac{1}{3}\Delta\varepsilon_p\mathbf{1} + \Delta\varepsilon_q\mathbf{n}^T\,, \qquad [9]$$

where $\Delta\varepsilon_p$ and $\Delta\varepsilon_q$ describe scalar rate quantities which are defined later on. The constitutive model used in this study is the damage model proposed by [ROU 89]. Here, the yield function taking ductile damage processes into account may is written as

$$\Phi = q - \underbrace{\sigma_0\left[\frac{\varepsilon^{pl}_{eqv}}{\sigma_0}E + 1\right]^{1/N}}_{\sigma^*} + B(\beta)D\exp(-\frac{p}{\sigma_1}) = 0\,, \qquad [10]$$

where σ^* represents the material hardening in terms of a power law, and the last part of [10] describes the damage (softening) behavior by the function $B(\beta)$ and an exponential assumption. Furthermore, E is YOUNGs modulus, σ_0 the initial yield stress, N the material hardening exponent, and D and σ_1 are *damage* material parameters. Note that the formulation of [10] in quantities p and q as functions of the KIRCHHOFF stress tensor $\boldsymbol{\tau}$ is comparable to the original formulation $F = \frac{\sigma_{eqv}}{\rho} + \ldots = 0$ in [ROU 89], because we can write $\frac{\sigma_{eqv}}{\rho} = \frac{\sigma_{eqv}}{\rho_0}J = \frac{q(\tau)}{\rho_0} = q$ for $\rho_0 = 1$ in the case of $\beta = 0$, see also comments of the authors to eqn. (17) in [ROU 89]. The function $B(\beta)$ is the *conjugate force* to the damage parameter β, defined by

$$B(\beta) = \frac{\sigma_1 f_0 \exp(\beta)}{1 - f_0 + f_0\exp(\beta)}\,. \qquad [11]$$

Here, the initial void volume fraction f_0 is the third damage depending material parameter used in this constitutive set of equations. The set of constitutive equations is complemented by the evolution equations for the plastic strain ε^{pl}_{eqv} and the damage parameter β. The macroscopic plastic strain rate $\dot{\boldsymbol{\epsilon}}^{pl}$ is determined by the classical associated flow rule

$$\dot{\boldsymbol{\epsilon}}^{pl} = \dot{\lambda}\frac{\partial\Phi}{\partial\boldsymbol{\tau}} = \dot{\lambda}\left\{\frac{\partial\Phi}{\partial q}\frac{\partial q}{\partial\boldsymbol{\tau}} + \frac{\partial\Phi}{\partial p}\frac{\partial p}{\partial\boldsymbol{\tau}}\right\}\,. \qquad [12]$$

Note that $\dot{\boldsymbol{\epsilon}}^{pl}$ coincides with the plastic increment $\Delta\boldsymbol{\epsilon}^{pl}$ for the algorithmic setting in [4] written in principal axes. The last bracket on the right hand side of [12] shows a further advantage of this formulation following [ARA 87], since it is very easy to determine the derivatives of Φ with respect to the scalar quantities q and p. One can see with [9] and [12] that

$$\Delta\varepsilon_p = -\dot{\lambda}\frac{\partial\Phi}{\partial p} \quad \text{and} \quad \Delta\varepsilon_q = \dot{\lambda}\frac{\partial\Phi}{\partial q}\,. \qquad [13]$$

These two equations allow the algebraic elimination of $\dot{\lambda}$ if

$$\Delta\varepsilon_p \frac{\partial \Phi}{\partial q} + \Delta\varepsilon_q \frac{\partial \Phi}{\partial p} = 0 \qquad [14]$$

is fulfilled. Thus, the increment of the plastic strain can be expressed by the two scalar quantities $\Delta\varepsilon_p$ and $\Delta\varepsilon_q$. Then the equivalent plastic strain ε^{pl}_{eqv} can be incremented directly by $\Delta\varepsilon_q$. The evolution equation for the damage parameter β is given by

$$\Delta\beta = \Delta\varepsilon_q D \exp(-\frac{p}{\sigma_1}) \qquad [15]$$

which is obviously dependent on the deviatoric part of the strain rate $\Delta\varepsilon_q$ and the actual hydrostatic pressure p. With this the whole set of constitutive equations is completed.

The evaluation of the material model for a given load level requires the solution of the three equations [10], [14] and [15] for the unknowns $\Delta\varepsilon_p$, $\Delta\varepsilon_q$ and $\Delta\beta$, respectively. *Classically* this evaluation would be done pointwise in the local level of the integrations points by an implicit EULER backward integration rule, which is described in the Appendix. In Section 2.2 we discussed a new approach, which allows for nonlocal formulation; its algorithmic treatment is shown in Section 4.2.

The exact linearization of the set of equations follows the description in [ARA 87]. At this point we just mention the starting point of the linearization

$$\boldsymbol{\tau} = \mathbf{C} : \left(\boldsymbol{\epsilon}^{tr} - \frac{1}{3}\Delta\varepsilon_p \mathbf{1} - \Delta\varepsilon_q \mathbf{n}^{\tau} \right) , \qquad [16]$$

where $\mathbf{C}$ is the elastic modulus defined by the LAMÉ constants. The variational expression for [16] is found as

$$\delta\boldsymbol{\tau} = \mathbf{C} : \left(\delta\boldsymbol{\epsilon}^{tr} - \frac{1}{3}\delta\Delta\varepsilon_p \mathbf{1} - \delta\Delta\varepsilon_q \mathbf{n}^{\tau} - \Delta\varepsilon_q \frac{\partial \mathbf{n}^{\tau}}{\partial \boldsymbol{\tau}} : \delta\boldsymbol{\tau} \right) . \qquad [17]$$

Some extended algebraic manipulations on [17], as described in [ARA 87], lead to the expressions $\delta\Delta\varepsilon_p$ and $\delta\Delta\varepsilon_q$ and finally to

$$\mathbf{D} = \left(\frac{\partial \boldsymbol{\tau}}{\partial \boldsymbol{\epsilon}} \right)_{t+\Delta t} , \qquad [18]$$

which is the material modulus for the implicit integration procedure at the end of the considered time interval $[t, t + \Delta t]$.

4. Finite element formulation

4.1. *3D–element*

Starting point is the weak form of equilibrium $g(\mathbf{u}, \delta\mathbf{u})$, see Fig. 1, formulated in the current configuration, where $\mathbf{u}$ is the displacement and $\mathbf{t}_L$ are the prescribed

tractions acting on the loaded boundary $\partial\mathcal{B}_\sigma$ of the body in the current configuration $\mathcal{B}$. Linearization with respect to the current deformation state, and rearrangement leads (with $\mathrm{d}v = J\,\mathrm{d}V$) to the following representation of the element stiffness

$$Dg^{elmt}(\hat{\mathbf{u}}, \delta\mathbf{u}) = \int_{\mathcal{B}_0} J\,(\Delta\boldsymbol{\sigma} + \mathrm{grad}\Delta\mathbf{u}\cdot\boldsymbol{\sigma}) : \mathrm{grad}\,\delta\mathbf{u}\;\mathrm{d}V^{elmt} \qquad [19]$$

where $J = \det\mathbf{F}$ and $\mathcal{B}_0$ denotes the reference configuration. As for the global resi-

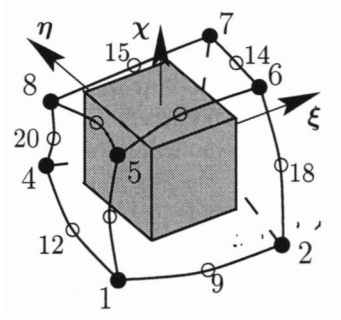

FIG. 2. *20–noded solid element*

duum vector resulting from $g(\mathbf{u}, \delta\mathbf{u})$ the elementwise results from [19] are assembled to the global stiffness matrix $\mathbf{K}$. For further explanations on the implementation of the consistent linearization of the used algorithm see [SIM 92] and the modifications in [REE 97] concerning the determination of the eigenvalue decomposition.

The discretization chosen in this paper is based on a 20–node–displacement element formulation with shape functions N_i, $(i = 1, 2, ..., 20)$, so that quadratic functions describe the element edges. Fig. 2 shows such an element in an arbitrary configuration. As in [MAT 94] we use a $2 \times 2 \times 2$–integration scheme, which means an *underintegration* with respect to the quadratic shape functions N_i. It shall be pointed out that again no *hourglassing* modes were detected like in the case of an 8–node–displacement element formulation and a $1 \times 1 \times 1$–integration scheme, see [BAA 98].

4.2. *The algorithmic treatment of the new approach*

As described above, the iterative solution procedure used for solving nonlinear problems by the finite element method requires an evaluation of the constitutive equations on the level of integration points. This is known as the lowest level of iteration in contrast to the global load/time incrementation and the subsequent *global* iteration fulfilling the weak form of equilibrium.

In our new approach the originally *local* evaluation of the set of constitutive equations on each integration point is shifted from the lowest level to a *global* solution while assembling the system stiffness matrix and the right hand side residual vector.

Instead of solving iteratively for each integration point on the element level, we assemble a large system of equations where the set of equations from each integration point enters blockwise along the main diagonal of the new system matrix, see also [BAA 00].

The global iteration scheme to find the current equilibrium requires in every iteration loop the assembling of the (global) system matrix and the right hand side vector. Parallel to this assembling procedure we solve the new global system of constitutive equations by an NEWTON–like iteration scheme. Due to the blockwise structure of the resulting system matrix it is possible to invert this matrix block–by–block and reassemble the resulting 3×3–submatrices for the use in the NEWTON–like iteration scheme. The character of a full JACOBIAN matrix for a *real* NEWTON scheme is lost because of the coupling of the quantities $\Delta\varepsilon_p$, $\Delta\varepsilon_q$ and $\Delta\beta$ through [1]. But this coupling is very weak in comparison to the dependence of the constitutive equations [20]–[22] in the local evaluation. So the rate of convergence is nearly quadratic as assumed for a full NEWTON scheme, see also time consumption in Table 2. Having determined the *nonlocal* results, the global stiffness and right hand side for the global equilibrium iteration can be assembled following the same scheme as for the classical solution technique.

5. Example and results

5.1. *Model of a CT specimen*

As example we examine a three dimensional model of a CT specimen discretized by 20–node solid elements as shown in Fig. 3. Due to symmetry just a quarter of

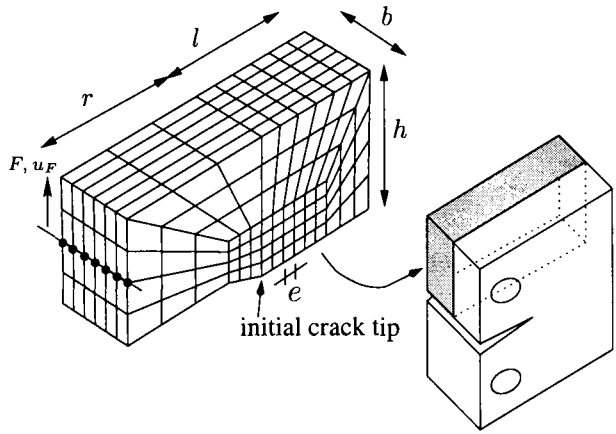

FIG. 3. *Model of CT specimen*

the structure is modeled, where the used edge lengths are shown in the right part of

Tab. 1. The loading is applied by the displacement u_F of the marked nodes and the respective nodes located in the middle of each element edge length, see Fig. 2 and Fig. 3. For simplicity applying an uniform numerical postprocessing procedure and for getting easier comparable results we just take the results of the marked nodes into account and sum up their reaction force to get a global answer of the structure. This proceeding can also be justified by the long distance between the loaded nodes and the zone of interest in front of the crack tip. So the resulting reaction forces on the loaded nodes are uniformly distributed and just scaled by a factor resulting from the quadratic shape functions along the loaded element edges. Here, we distinguish two different mesh types named by the typical element edge length e in front of the crack tip. The first mesh is characterized by $e = 1.0$ mm, the other one by $e = 0.5$ mm. The set of material parameters used is shown in Tab. 1, where the first four parameters

E	ν	σ_0	N	D	σ_1	f_0	f_F	r	l	b	h
210000	0.2	460	7	3	300	0.01	0.19	6	5	3	5

TAB. 1. *Material parameters, stress dimension [MPa], and geometry in [mm]*

can be obtained by simple tensile tests, and D, σ_1 and f_0 are responsible for the damage representation of the constitutive model. Ductile crack growth is represented by reaching the threshold value of $f_F = 0.19$ by the local value of the volume fraction f expressed in terms of the damage parameter β by $f = \frac{B(\beta)}{\sigma_1}$, see Eqn. [11], in any integration point. This final value f_F as threshold for the evolution of f is *not* urgent in this formulation using the ROUSSELIER damage model and its damage parameter β, but in order to get comparable results to the use of e.g. the GURSON damage model, see e.g. [BAA 98], it is very attractive. The maximum distance of the respective integration points from the initial crack tip defines the actual crack growth Δa. To show the effect of the nonlocal regularization technique introduced here, the *characteristic* length scale is fixed to $l_c = 1.0$ mm for the two different mesh types. So l_c corresponds to the coarse discretization with $e = 1.0$ mm.

5.2. *Results*

The response of the nodal reaction force vs. the applied displacement u_F is plotted in Fig. 4. It can be seen from the curves (1) and (3) that the 3D model behaves in the usual way depending on the discretization for the traditional local approach with $l_c \equiv 0.0$ mm. The finer the used FE mesh is, the earlier the onset of strain localization is reached. Afterwards the negative slope of the respective curves gets steeper with increasing refinement of the discretization.

In contrast to these *classical* mesh sensitive results, the responses of the nonlocal approaches show a different behavior for the two types of discretization. Although the typical element edge length e is varied from $e = 0.5$ mm to $e = 1.0$ mm, the curves (2) and (4) characterizes nearly the same behavior of the regularized calculations with

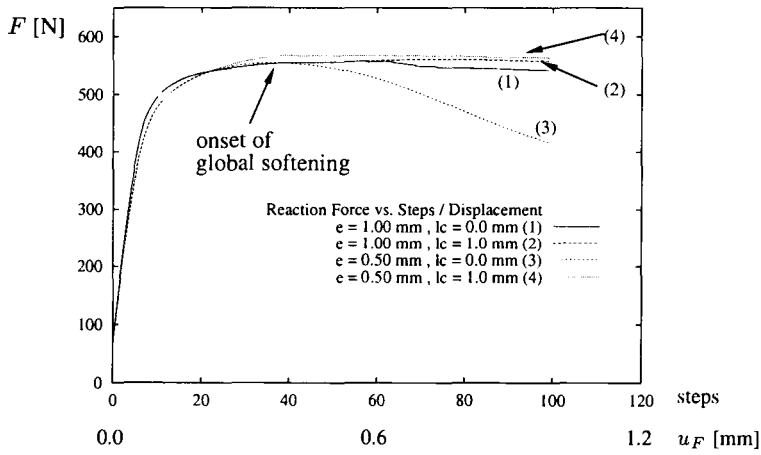

FIG. 4. *Reaction force vs. end displacement for different discretization*

the identical internal length $l_c = 1.0$ mm, while the onset of global softening can be observed for all curves at a displacement of about $u_F = 0.38$ mm on the loaded nodes. Fig. 5 represents the maximum values for the void volume fraction f in the first integration point in front of the initial crack tip in the center of the specimen vs. the number of load steps. These values are plotted for the cases (2), (3) and (4) to show the effect of the regularization technique. In addition, the threshold value of $f_F = 0.19$ is marked by a dashed line indicating the transition of this value by the different calculations at different load steps. The crack advance Δa, which corresponds to this maximal value of f in the front of the crack tip, is marked by dots in the plot. This shows that the local analysis (3) responses with a larger crack advance of $\Delta a \simeq 1.7$ mm at load step 90, while the nonlocal representations (2) and (4) for both discretization result in a crack growth of about $\Delta a \simeq 0.8$ mm (the accurate position of the respective integration points varies due to the different element edge lengths in front of the crack tip) at this load step 90. So, these regularized results show nearly the same crack advance, although different discretizations are used. Tab. 2 shows

	DOF	Time : Equiv. Inv.	Time : gbl. NLoc
$e = 1.0$ mm	850	0.08 secs.	0.61 secs.
$e = 0.5$ mm	7545	8.5 secs.	10.1 secs.

TAB. 2. *Comparison of computational costs iterating the global equilibrium at load level 71*

a comparison of time consumption for calculations with two different discretizations $e = 1.0$ mm and $e = 0.5$ mm and the resulting *Degrees Of Freedom*. The third column shows the time for inverting the FE system matrix by an advanced GAUSS elimination during the iteration of the equilibrium state on an *IBM RS6000/397* workstation. Wi-

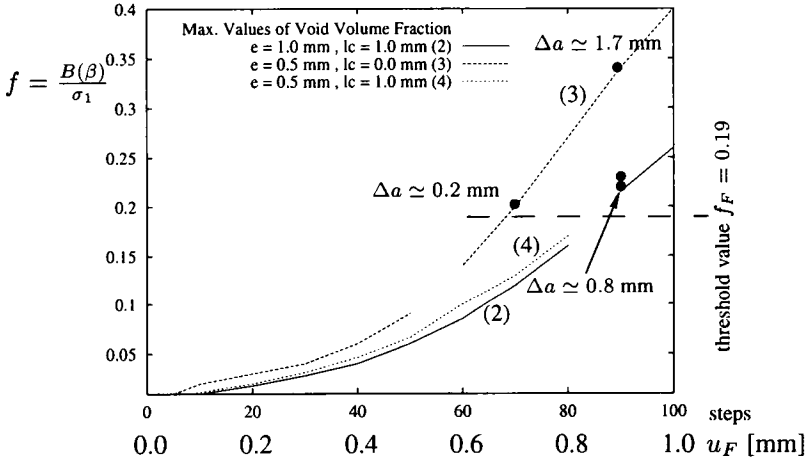

FIG. 5. *Maximum values of* $f = \frac{B(\beta)}{\sigma_1}$ *in the center of the specimen*

thin the considered load level of step 71 about seven iteration steps are needed to reach a converged situation. This time consumption is independent from the *local* or *nonlocal* evaluation procedure. The last column represents the duration for solving the set of constitutive equations on the global level within the proposed *nonlocal* approach. The *classicaly local* solution needs —in contrast to that— a vanishing time to assemble the FE stiffness matrix, indeed without nonlocal smoothing. So one can see, that the time consumption for solving the *nonlocal system* increases obviously with increasing number of integration points, but the amount of time is in tolerable limits respecting the profit of a nonlocal evaluation. These first results for the application of a new nonlocal solution approach demonstrate the capability of this technique in smoothing the classically local results on the level of integration points to a nonlocal distribution of the damage parameter β, which is responsible for the softening behavior of a structure. In this sense it can be seen, that the applied modification of the classical FE solution approach, shifting the level of iteration of the constitutive equations to a more global, spatially dependent one, effects the structural response of a loaded specimen. Keeping these results in mind, an attractive future work could be a modification of the classical FE solution approach with respect to a useful possibility to enable a "communication" between the integration points depending on their spatial position.

6. Summary

In this contribution we show a study of a 3D simulation of CT specimen using the ROUSSELIER damage model combined with a 3–dimensional finite element formulation based on 20–node–solid elements. The main attention is put to a new algorithmic

approach to the iteration of the constitutive equations applying a nonlocal regularization to avoid mesh sensitive results.

The first results for this treatment are shown here and underline the algorithmic applicability of the new approach. The additional time consumption for the nonlocal evaluation is in tolerable limits, although some further investigation concerning a faster realization of the new approach have to follow. Studies especially about the calibration of the model to experimental data are in preparation.

7. Bibliography

[ARA 87] ARAVAS N., « On the numerical Integration of a Class of pressure–dependent Plasticity Models », *International Journal for Numerical Methods in Engineering*, vol. 24, 1987, p. 1395–1416.

[BAA 97] BAASER H., HOHE J., GROSS D., « Ductile crack growth analysis using the Gurson damage model », KOSINSKI W., DE BOER R., GROSS D., Eds., *Problems of Environmental and Damage Mechanics*, n° ISBN 83-906354-1-0, Warszawa, Poland, 1997, p. 139–147.

[BAA 00] BAASER H., TVERGAARD V., « A New Algorithmic Approach treating Nonlocal Effects at Finite Rate-independent Deformation using the ROUSSELIER Damage Model », *submitted to Computer Methods in Applied Mechanics and Engineering*, , 2000, see also DCAMM Report 647, TU Denmark, Lyngby.

[BAA 98] BAASER H., GROSS D., « Damage and Strain Localisation during Crack Propagation in Thin–Walled Shells », BERTRAM A., SIDOROFF F., Eds., *Mechanics of Materials with Intrinsic Length Scale*, n° ISBN 2-86883-388-8, Magdeburg, Germany, 1998A, EDP Sciences, p. 13–17, Journal de Physique IV, **8**.

[BAŽ 88] BAŽANT Z., PIJAUDIER-CABOT G., « Nonlocal Continuum Damage, Localisation Instability and Convergence », *Journal of Applied Mechanics*, vol. 55, 1988, p. 287–293.

[BOR 99] DE BORST R., PAMIN J., GEERS M., « On coupled gradient–dependent plasticity and damage theories with a view to localization analysis », *European Journal of Mechanics - A/Solids*, vol. 18, 1999, p. 939–962.

[EHL 98] EHLERS W., DIEBELS S., VOLK W., « Deformation and Compatibility for Elasto–plastic Micropolar Materials with Applications to Geomechanical Problems », BERTRAM A., FOREST S., SIDOROFF F., Eds., *Mechanics of Materials with Intrinsic Length Scale*, Magdeburg, Germany, 1998, p. 120–127.

[HOH 96] HOHE J., BAASER H., GROSS D., « Analysis of ductile crack growth by means of a cohesive damage model », *International Journal of Fracture*, vol. 81, 1996, p. 99–112.

[LEB 94] LEBLOND J., PERRIN G., DEVAUX J., « Bifurcation Effects in Ductile Metals with Nonlocal Damage », *ASME Journal of Applied Mechanics*, vol. 61, 1994, p. 236–242.

[LI 94] LI Z., BILBY B., HOWARD I., « A study of the internal parameters of ductile damage theory », *Fatigue & Fracture of Engineering Materials & Structures*, vol. 17, n° 9, 1994, p. 1075–1087.

[MAT 94] MATHUR K., NEEDLEMAN A., TVERGAARD V., « Ductile failure analyses on massively parallel computers », *Computer Methods in Applied Mechanics and Engineering*, vol. 119, 1994, p. 283–309.

[OLI 96] OLIVER J., « Modelling strong Discontinuities in Solid Mechanics via Strain Softening Constitutive Equations : Part I and II », *International Journal for Numerical Methods in Engineering*, vol. 39, 1996, p. 3575–3623.

[PIJ 93] PIJAUDIER-CABOT G., BENALLAL A., « Strain localization and bifurcation in a nonlocal continuum », *International Journal of Solids and Structures*, vol. 30, n° 13, 1993, p. 1761–1775.

[REE 97] REESE S., WRIGGERS P., « A material model for rubber–like polymers exhibiting plastic deformation : computational aspects and a comparison with experimental results », *Computer Methods in Applied Mechanics and Engineering*, vol. 148, 1997, p. 279–298.

[ROU 89] ROUSSELIER G., DEVAUX J.-C., MOTTET G., DEVESA G., « A Methodology for Ductile Fracture Analysis based on Damage Mechanics : An Illustration of a Local Approach of Fracture », *Nonlinear Fracture Mechanics*, vol. 2, 1989, p. 332–354.

[SIM 92] SIMO J., « Algorithms for Static and Dynamic Multiplicative Plasticity that preserve the classical Return Mapping Schemes of the infinitesimal Theory », *Computer Methods in Applied Mechanics and Engineering*, vol. 99, 1992, p. 61–112.

[TVE 89] TVERGAARD V., « Material Failure by Void Growth to Coalescence », *Advances in Applied Mechanics*, vol. 27, 1989, p. 83–151.

[TVE 97] TVERGAARD V., NEEDLEMAN A., « Nonlocal Effects on Localization in a Void–Sheet », *International Journal of Solids and Structures*, vol. 34, n° 18, 1997, p. 2221–2238.

Appendix : Iteration of the set of constitutive equations

The unknowns $\Delta\varepsilon_p$, $\Delta\varepsilon_q$ and $\Delta\beta$ are determined by a NEWTON–like iteration scheme. The elastic *trial*–stress state is determined as described in Section 3.1, where also the quantities p^{tr} and q^{tr} are obtained as described below [8]. The "return mapping" iteration described here is carried out for integration points violating the yield condition [10], either on the local level or as shown in Sections 2.2 and 4.2 with the new global algorithm.

$$r_1 = \frac{1}{E}\left\{ q - \sigma_0 \left[\frac{\varepsilon_{equ}^{pl}}{\sigma_0} E + 1 \right]^{1/N} + B(\beta^{\mathrm{loc/nonl}}) D \exp(-\frac{p}{\sigma_1}) \right\} \quad [20]$$

$$r_2 = \Delta\varepsilon_p \frac{\partial\Phi}{\partial q} + \Delta\varepsilon_q \frac{\partial\Phi}{\partial p} = 0 \quad [21]$$

$$r_3 = \Delta\beta^{\mathrm{loc/nonl}} - \Delta\varepsilon_q D \exp(-\frac{p}{\sigma_1}) = 0 \quad [22]$$

For having a better *condition* of the iteration system the function r_1 is weighted by YOUNGs modulus, so that a dimensionless expression results as for r_2 and r_3.
Evaluate for $i, j = 1, 2, 3$

$$\mathbf{x}^{k+1} = \mathbf{x}^k - \Delta\mathbf{x} \quad [23]$$

where $\Delta\mathbf{x}$ is either calculated directly on each integration point by $\Delta x_i = J_{ij}^{-1} r_j$ or calculated using a global iteration scheme where the nonlocal smoothing [1] is applied after *every* iteration step as described in the previous sections. So one gets $[x_1, x_2, x_3]^{\mathrm{T}} = [\Delta\varepsilon_p, \Delta\varepsilon_q, \Delta\beta]^{\mathrm{T}}$. The quantities $\varepsilon_{equ}^{pl,tr}$ and β^{tr} are used to store the accumulated *history* of the actual integration point in addition to the tensorial quantity needed in [7].